



Al-Rafidain Journal of Engineering Sciences

Journal homepage <https://rjes.iq/index.php/rjes>

ISSN 3005-3153 (Online)



Heat Transfer and Pressure Drop in Plate Fin Heat Exchangers: A Numerical Approach

Ali Hameed Hasan¹, Salem Mehrzad Banooni¹, Laith Jaafer Habeeb^{2,*}

¹Mechanical Engineering Department, Faculty of Engineering, Shahid Chamran University of Ahvaz, Ahvaz, Khuzestan Province, Iran. alihamedhassan574@gmail.com, banooni@scu.ar.ir

²Training and Workshop Center, University of Technology – Iraq, Baghdad, Iraq, Laith.J.Habeeb@uotechnology.edu.iq

ARTICLE INFO

Article history:

Received 03 January 2024
Revised 05 January 2024
Accepted 10 January 2024
Available online 10 January 2024

Keywords:

Heat Transfer
Plate Fin Heat Exchangers
Numerical Approach

ABSTRACT

An apparatus for transferring thermal energy across an impermeable barrier between two or more fluids is a heat exchanger. The effective transmission of heat from a hot fluid to a cold fluid is its primary goal. The temperature differential between the two fluids directly affects this heat transfer. Using CFD study with FLUENT 2020 R1, the performance characteristics of the compact plate fin heat exchanger's improved surfaces are examined. The simulation of heat transfer and flow encompassed a variety of velocities including completely turbulent regions. The pressure, temperature, and velocity contours were taken from the Fluent simulations. To determine the heat exchanger's flow and heat transfer performance, numerical analysis has been done. Since boundary conditions are crucial to CFD, they have been carefully chosen. The flow field, heat transfer, thickness, and wavelength were all predicted using the software code for a range of air to water velocities. Three distinct wavelengths of numerical simulations for a plate-fin heat exchanger were used in the study (10, 20, and 30). There were changes to the fin thickness, entry locations, and air and water entry velocities. Solid Works and Ansys were used to create the geometry for the three-level fin models that were placed inside the heat exchanger, both with and without a cover. For determining the heat exchanger's geometry and fin isometry, three levels measuring 19.6 mm in height and 53.64 mm in width were constructed. The fins have a thickness of 0.2 to 0.4 mm. As the air and water velocities vary, so does the temperature inside the heat exchanger. Because the topmost layer is a warm stream's flow channel, the temperature rises there, whereas the opposite effect is seen close to the bottom layer. Convection heat transmission to the surroundings and conduction heat transfer through the heat exchanger's side plates are the causes of fluid temperature fluctuations in the depth direction.

1. Introduction

Heat exchangers are a crucial component of many different engineering systems and plants. Because of this, heat exchanger architecture and design are frequently essential to the efficient running of such a system. In contrast, the weight and volume of the heat exchangers in cars and airplanes should be as low as feasible for a given heat transfer. Therefore, the ability of a heat exchanger to transmit the

required amount of heat efficiently is the most crucial criterion.

By using holographic interferometry, Fehle et al. [1] discovered the behavior of heat transport in the consolidated plate-fin heat exchanger. He made the temperature field visible in a non-invasive, inertia-less manner in order to achieve this. He then determines the local Nusselt number from the line of constant temperature at the temperature field's wall. They examined the heat transfer in-plane fin

* Corresponding author E-mail address: Laith.J.Habeeb@uotechnology.edu.iq
<https://doi.org/10.61268/qe48kc51>

This work is an open-access article distributed under a CC BY license (Creative Commons Attribution 4.0 International) under

<https://creativecommons.org/licenses/by-nc-sa/4.0/>

arrangements before computing the impact of the hot metal sheets' corner radii. Additionally, they looked at how circular segments in inclined, non-staggered, and staggered patterns produced turbulence. They discovered that the non-staggered geometry has the maximum rate of heat transfer, whereas the staggering geometry has the best volume goodness factor after computing the median Nusselt number. Using the limited element technique, Ranganayakulu et al. [2] examined the heat exchangers with cross-flow plate-fin, cross-flow tube fin, parallel plate-fin, and counter-flow plate-fin configurations, considering the impact of heat conduction along the heat exchanger wall in a linear direction. It is observed that in every scenario, the rendering deviation of cross-flow heat exchangers is greater than that of counter-flow and parallel flow heat exchangers. The temperature distribution appears to be two-dimensional. Given a thermal model and the best conditions, Hajabdollahi et al. [3] built a small heat exchanger. The five design parameters are the fin pitch, fin height, cold stream flow length, no-flow length, and hot stream flow length. Utilizing CFD analysis in conjunction with an ANN (Artificial Neural Network), they improved the relationship between the Fanning friction factor and the Colburn factor (J) (f).

The plate-fin exchanger's dynamic and steady-state simulations were carried out by Pingaud et al. [4]. They created an algorithm for multi-fluid and multi-passages PFHEs for both the steady-state and transient simulations by using modeling based on the mass, momentum, and energy balances. They used an underlying integration approach to solve the model equations including partial differentiation and to cure the counter-current flow. Menzel and Hecht [5] discovered that liquid logging present on the heat exchanger surfaces and sluggish flow reflected two-phase up-flow in PFHEs both lower heat exchanger performance. In order to provide private treatment, they selected fluid combinations with a wide boiling range that evaporate at high NTU values at relatively modest gas fluxes. A greater gas mass flux is required for the flow condition of non-refluxes, which results in a

higher pressure drop. Dubrovsky [6] studied a novel convective heat transfer increase rule for PFHE surfaces. When compared to vortex-promoted heat transfer surfaces with an equivalent small channel at the same Reynolds numbers, this is characterized by $(\zeta/\zeta_{sm}) \leq (Nu/Nu_{sm})$. Dubrovsky created heat exchanger cores with three distinct fin surfaces. Two of the three surfaces feature offset channels with equilateral triangular and rectangular cross sections, while the third surface has isosceles triangular cross sections with transverse grooves that extend along the length of the channel. Using the finite element method, Ranganayakulu et al. [7] examined the impact of non-uniform flow distribution of two-dimensional inlet fluids of both the hot and cold sides of the fluid in a cross-flow PFHE. They created mathematical formulas for a variety of mal-distribution models that account for the efficacy of the exchanger and its declination as a result of non-uniform flow in all design and operating condition ranges. Kundu and Das [8] established the ideal fin dimensions for heat exchangers of the fin tube type. For a fixed fin volume, they calculated the maximal heat dissipation for a particular value of thickness or pitch length. Averous et al. (1999) gave a brazed plate heat exchanger dynamic simulation. Ranganayakulu et al. [9] used the finite element approach to study the cross flow compact PFHE while taking into consideration the combined impacts of 2D heat conduction in the longitudinal direction through the exchanger wall, non-uniform fluid flow in the inlet, and temperature distribution. Taking into account heat conduction in the longitudinal direction, non-uniformity of the flow, and non-uniformity of the temperature, they found that the declination of the thermal performance promotes the elimination of each other in the areas of higher NTU but promotes each other in the areas of lower NTU.

The primary goal of the compact plate fin heat exchangers designed by Picon-Nunez et al. [10] was to make use of the pressure drop. The surface is chosen based on the volume performance index's (VPI) performance. The type of surface on each side of the streams that participates in the heat transfer process must be

specified for the purpose of PFHE sizing. Thus, the primary goal of the design was to have a minimal exchanger volume. They came to the conclusion that this might be accomplished by using the steam pressure drop and creating extremely thermally efficient heat transfer surfaces. Wen & Li [11] examined the fluid flow distribution performance in the PFHE headers. They discovered that, as a result of inadequate header configuration, the fluid flow mal-distribution in the header length direction of industrial convectional headers is extremely severe. They also discovered that the flow absolute parameter can be decreased by employing baffles. A model for understanding the flow behavior in plate fin and tube fin heat exchangers—which consist of two parallel plates with a single cylinder positioned in the space between the plates—was presented by Şahin et al. [12]. They conducted their experiment with a Re value of 4000–7500 and a duct height to cylinder dia. ratio of 0.365. Peng and Ling [13] as a way to anticipate the properties of heat transfer and pressure drop in plate fin heat exchangers introduced artificial neural networks, or ANNs. According to the estimated result, ANN models can be utilized to provide accurate estimates of the friction factor (f) and Colburn factor (j) in PFHEs. In order to better understand the impact of convection on compact heat exchangers with rectangular offset strip fins, Manglik and Bergles [14] looked into the thermodynamic and hydraulic design tools. The j and f data for the real cores were reanalyzed, and the asymptotic behavior in the totally turbulent and extreme laminar flow regimes was also determined. The asymptotes derived from the power law expressions were associated with the dimensionless geometric parameters α , δ , and γ , as well as the Reynolds number (Re). Ultimately, they created formulas for j and f data in regimes of laminar, turbulent, and transitional flow.

Mishra et al. [15] created a genetic algorithm-based optimization method. The primary goal is to minimize the creation of entropy for a particular heat obligation within predetermined spatial constraints. According to Ismail et al. [16], the thermodynamic design of compact

heat exchangers is significantly influenced by the computed dimensional performance of the heat transfer surfaces (j and f vs. Re). Using the Fluent software, they examined the flow patterns of 16 different types of wavy fins and three types of offset fins. Suzuki et al. [17] investigated the flow properties and heat transfer of a 2D flat plate employed in a mixed (free flow) convection zone at low Reynolds number using computational and experimental study. Youcef-Ali [18] made use of air's low thermophysical properties to transmit heat in solar collectors. By doing this, the fluid and absorber plate's thermal heat transmission is encouraged. This improves the solar collector's thermal performance. In an experiment, Fishedick et al. [19] investigated the heat recovery of a ceramic PFHE used in heat exchanger applications.

Using CFD study with FLUENT 2020 R1, the performance characteristics of the compact plate fin heat exchanger's improved surfaces are examined. Data from earlier research is used to validate the CFD predictions. The three-dimensional fin flow channel's geometrical aspects are described by the fin characteristics. A range of velocity, completely turbulent regions of heat transfer and flow were produced by simulating the flow and temperature fields in plate fin heat exchanger passages. The pressure, temperature, and velocity contours were taken from the Fluent simulations.

1. CFD Analysis

Three values (0.2, 0.3, and 0.4) mm will be altered in the fin thickness during the simulation process, and a plate fin heat exchanger with various wavelengths (10, 20, and 30) will be used to measure temperature and pressure variations. Three ratios of air to water velocities (0.1, 0.2, and 0.3) will be used, which will alter the velocity of entrance of both water and air used in the study. Water will enter from the middle, and in the second scenario, the air will enter from the top and bottom. These changes will also affect the locations where water and air enter.

For CFD analysis, the following data is needed:

- a grid of points where the variables determined by CFD can be stored.
- Boundary conditions that are necessary to specify every condition at the flow domain's borders and that make it possible to compute the boundary values of every variable.
- characteristics of a fluid, including density, viscosity, and thermal conductivity.
- flow models that outline the different characteristics of the flow, including mass, heat transmission, and turbulence.
- In both steady state and transient simulations, initial circumstances are

employed to offer a rough estimate of the solution variables.

- The numerical solution process's behavior must be regulated by the solver's control settings.

1.1 Geometry

SoildWorks was utilized to construct the geometry, while Ansys Fluent was utilized for the simulations. Geometry in three dimensions was produced. Figure (1) illustrates the top view of the wavelength difference of the fins using the three wavelengths (10, 20, and 30). The fins within the heat exchanger, both with and without a cover, are depicted in Figure (3). Each level measures 19.6 mm in height and 53.64 mm in width. Fin thickness is measured in three different values: 0.2, 0.3, and 0.4 mm

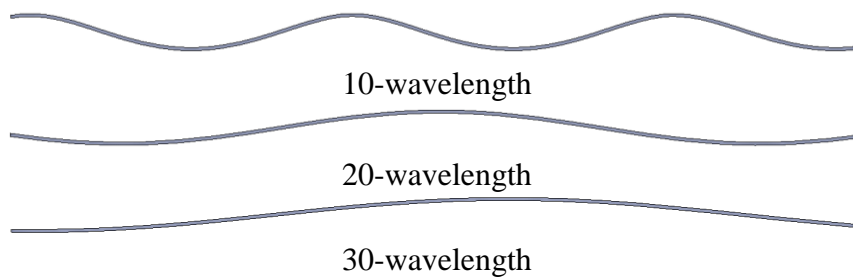


Figure 1: Top view of the heat exchanger fins.

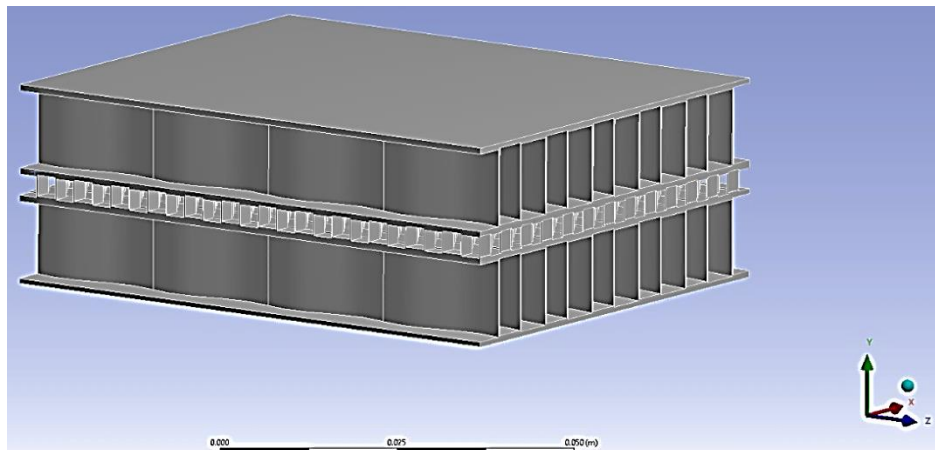


Figure 2: Geometry of the heat exchanger.

1.2. Mesh

The process of breaking the domain up into smaller components is called grid generation. Various varieties of grids exist, such as

prisms, tetrahedral, and hexahedral, depending on how the elements are shaped. A mesh that fits the bounds of the computational region is necessary for standard CFD algorithms. Extensive study has always been conducted on

the production of computational mesh appropriate for the discretized solution of three-dimensional conservation energy, continuity, momentum, and energy equations. The precision and stability of the numerical computation are highly dependent on the mesh quality. No matter what kind of mesh is utilized in the domain, it is imperative to verify its quality. Ansys Fluent gives us the ability to examine a crucial mesh quality metric known as the orthogonal quality.

• Mesh Validation

One of the most crucial phases in the finite element analysis is creating the mesh. The

entire numerical research will depend on the kind of mesh that is used and the size of the mesh cells. Various mesh sizes were employed to validate the mesh used in these experiments [20]. The four mesh cases that were examined are displayed in Table 1. Each case's output temperature for the model was determined, as indicated in the table (1). In cases three and four, the water's exit temperature appears to be stable as the number of components and nodes rises. A picture of the meshed fins and geometry is shown in Figure (3).

Table (1) Mesh validation characteristics.

Case	Node	Element	Maximum temperature (K)
1	623434	634533	329.5
2	734503	724453	325.6
3	856634	834553	324.7
4	905030	951074	324.5

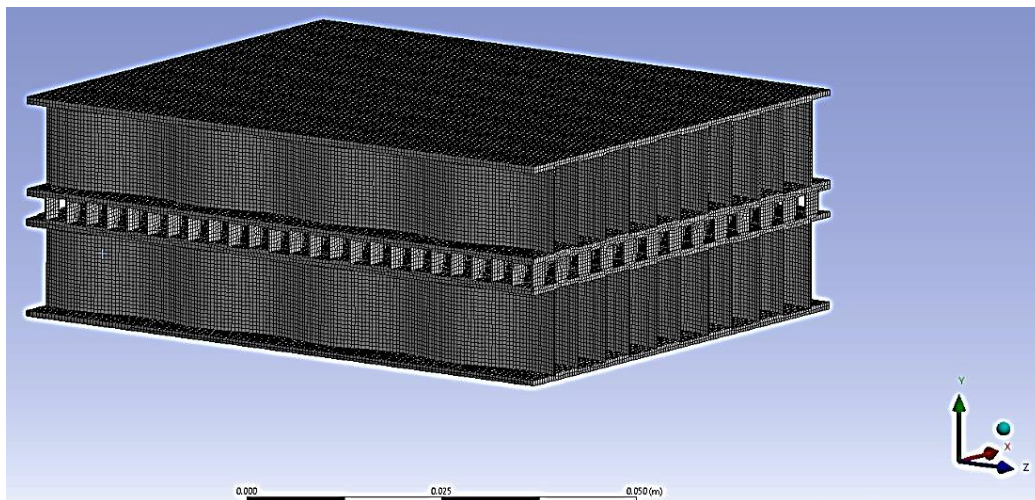


Figure 3: Mesh used in the simulations.

Three cell zones made up the model; the solid zones represented the fins, while the fluid zones represented the water and air. Air would flow in the outside two edges, while water would flow in the center. A variety of scenarios were simulated, with water flowing in the endless two sides and air flowing in the center. The air-to-water velocity ratio

fluctuates throughout (0.1, 0.2, and 0.3). The air symbolizes a cold fluid at 20 °C, while water is a hot fluid at 50 °C. In the simulations, the k-epsilon turbulent model was combined with the steady state model. There were 1000 iterations in the simulations. The tested temperatures and velocities for each fluid are displayed in Table (2).

Table (2) Cases that was tested.

Case	Velocity Water	Temperature Water	Velocity Air	Temperature Air
1	0.1	25	1	50
2	0.15	25	1	50
3	0.2	25	1	50
4	0.1	50	1	25
5	0.15	50	1	25
6	0.2	50	1	25
7	0.1	25	3	50
8	0.15	25	3	50
9	0.2	25	3	50
10	0.1	50	3	25
11	0.15	50	3	25
12	0.2	50	3	25
13	0.1	25	5	50
14	0.15	25	5	50
15	0.2	25	5	50
16	0.1	50	5	25
17	0.15	50	5	25
18	0.2	50	5	25

2. Design Calculation

The following parameters are estimated as part of the basic design of plate fin heat exchangers.

• Heat Transfer Rate

Heat transfer rate through the inner side is:

$$Q_h = \dot{m}_h C_{p_h} (T_{ho} - T_{hi}) \quad (1)$$

The temperature differential on the water side of the equation is used to compute the heat dissipation during this investigation (2). This is a result of the precise parameter measurement in this area.

• Inner Side Heat Transfer Coefficient

Newton's rule of cooling allows for the computation of the inner side heat transfer coefficient, which is:

$$Q_h = h_i A_i (T_m - T_s) \quad (2)$$

where:

$$T_m = \frac{T_{hi} + T_{ho}}{2} \quad (3)$$

$$T_s = \frac{T_1 + \dots + T_7}{7} \quad (4)$$

Then Nusselt number for the inner surface can be calculated as follows:

$$Nu = \frac{h_i d_i}{k_h} \quad (5)$$

3. Turbulence Model

Three methods for the k-epsilon turbulence model in the multiphase flow are provided by Ansys Fluent:

1. Model of Turbulence Mixture
2. Model with distributed turbulence
3. Model of turbulence at every stage

These equations can be used to define the two and three phases fluidized bed model, for which the turbulence RNG mixing model was configured (Fluent User's Guide).

$$\begin{aligned} \frac{\partial}{\partial t} (\rho_m k) + \nabla \cdot (\rho_m \vec{v}_m k) &= \nabla \cdot \left(\frac{\mu_{t,m}}{\sigma k} \nabla k \right) + G_{k,m} - \rho_m \epsilon \\ \nabla \cdot \left(\frac{\mu_{t,m}}{\sigma k} \nabla k \right) + G_{k,m} - \rho_m \epsilon &= \end{aligned} \quad (6)$$

$$\begin{aligned} \frac{\partial}{\partial t} (\rho_m \epsilon) + \nabla \cdot (\rho_m \vec{v}_m \epsilon) &= \nabla \cdot \left(\frac{\mu_{t,m}}{\sigma_\epsilon} \nabla \epsilon \right) + \frac{\epsilon}{k} (C_{1\epsilon} G_{k,m} - C_{2\epsilon} \rho_m \epsilon) \\ \nabla \cdot (\rho_m \vec{v}_m \epsilon) &= \nabla \cdot \left(\frac{\mu_{t,m}}{\sigma_\epsilon} \nabla \epsilon \right) + \frac{\epsilon}{k} (C_{1\epsilon} G_{k,m} - C_{2\epsilon} \rho_m \epsilon) \end{aligned} \quad (7)$$

Where ϵ is the turbulent dissipation rate, G is the energy, σ and is the surface tension.

Equations (8) and (9), respectively, can be used to find the mixture's density and velocity.

$$\rho_m = \sum_{i=1}^N \alpha_i \rho_i \rho_m = \sum_{i=1}^N \alpha_i \rho_i \quad (8)$$

$$\vec{v}_m = \frac{\sum_{i=1}^N \alpha_i \rho_i \vec{v}_i}{\sum_{i=1}^N \alpha_i \rho_i} \quad (9)$$

Equations (10) and (11) can be used to find the mixture's turbulent viscosity and kinetic energy, respectively.

$$\mu_{t,m} = \rho_m C_m \frac{k^2}{\epsilon} \mu_{t,m} = \rho_m C_m \frac{k^2}{\epsilon} \quad (10)$$

$$G_{k,m} = \mu_{t,m} (\nabla \vec{v}_m + (\nabla \vec{v}_m)^T) : \nabla \vec{v}_m \quad (11)$$

The Finite Volume Method was used to solve the governing conservation equations in order to do the numerical computation. The well-known SIMPLE algorithm method for numerical computations is used to obtain the pressure-velocity coupling in the governing equations. The boundary conditions have been carefully chosen because, in computational fluid dynamics, the settings are crucial. Initially, numerical analysis was done using the three ratios of air to water velocity for the fins' first thickness and wavelength. Later, the three air to water velocity measurements were also used to study the fins' second thickness and wavelength. The performance of the heat exchanger's flow and heat transfer was forecast using the commercial CFD application Fluent code. ANSYS-Workbench Fluent was used for the numerical simulation of the current heat exchanger in order to forecast the flow field, heat transfer for various air to water velocity values, fin thickness, and fin wavelength [21].

4. Results and Discussion

Plate fin heat exchanger was studied numerically using FLUENT 2020 R1 . The fin height (h), fin spacing (s), fin thickness (t), diameter of the perforation (d), number of holes per inch length, spacing between the perforations and fin length (l), describe the geometrical features of the three-dimensional fin flow channel. From the numerical model the contours of the pressure, temperature, and velocity inside the heat exchanger was obtained. The values of water velocity, water

temperature, air velocity, and air temperature changed with each simulated study.

4.1 Temperature Distribution

The heat exchanger's temperature contours as a function of water velocity are displayed in Figures (4) through (11). The figure depicts the thermal distribution of the fluid flow within the stream that parallels the flow plate fin heat exchanger and includes heat leakage. As may be observed, the heat exchanger's depth direction, or x direction, exhibits an uneven temperature distribution. Convection heat transmission to the surroundings and conduction heat transfer through the heat exchanger's side plates are the causes of fluid temperature fluctuations in the depth direction. The temperature distribution of the solid matrix in the side plates and the heat exchanger's Y-Z vertical cross-section is shown in Figures. The temperature difference in the side plate's transverse direction (along Z) is negligible, as seen in the aforementioned figure, but it is large in the Y-Z vertical cross-section along the Z direction. Convective heat transfer between the fluid in the channels and the solid matrix is the cause of this temperature change. The temperature distribution of the solid matrix is shown transversely in Figures.

It is believed that different layers in a stream have similar properties, such as mass flow rate, inlet temperature and pressure, fin type and dimensions, and so forth, in order to study the impact of the number of layers. In general, efficacy rises and entropy generation per unit cell falls as the number of unit cells increases. This is because, in the case of a small number of layers, the boundary conditions have a substantial impact on the fluid temperature. Boundary circumstances have less of an impact on the bulk stream temperature as the number of layers rises. The red line in the aforementioned figure shows the results of the simulation with periodic boundary conditions. The solution converges to the periodic boundary conditions as the number of layers increases. Figures demonstrated that compared to an adiabatic heat exchanger, the thermal efficacy and entropy generation in a heat

exchanger with heat leakage are more sensitive to the number of unit cells.

The temperature distribution in the channel length direction at the computational domain's surface and in the sections of the x-z planes. It is evident that cold fluid enters the top channel at a temperature of 300 K and is heated along the channel length, whereas hot fluid, with a

uniform temperature of 330 K, enters the channel and is cooled along its length. The channel barriers allow heat to be transferred between the two channels. Heat radiates from the walls, which act as a medium for the heat exchange between fluids and heat, as seen in Figures.

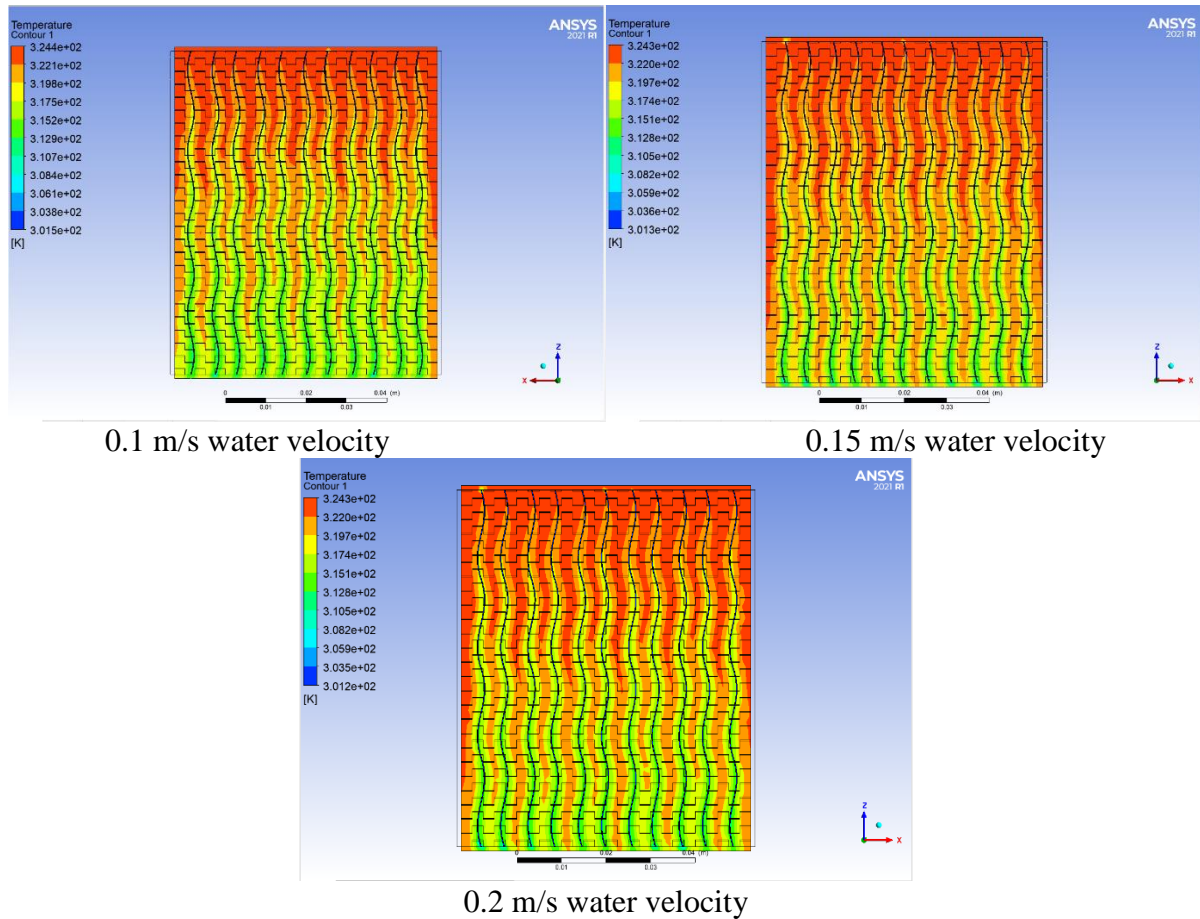


Figure 4: Temperature contours for heat exchanger using 25 oC water temperature, 3 m/s air velocity, 50 oC air temperature, and different values of water velocities.

Figures display the average channel fluid temperatures along the direction of the channel length. The temperature fields have been projected to a one-dimensional average temperature along the channel length direction using the General Projection functions. Since a significantly higher heat capacity rate is used

for the cold fluid, the average temperature drop for the hot fluid is higher than that of the water. The fluid would considerably cool if the channel length were extended, although the temperature would not rise much. Figures also display the average temperatures of the hot and cold fluids at the channel exits.

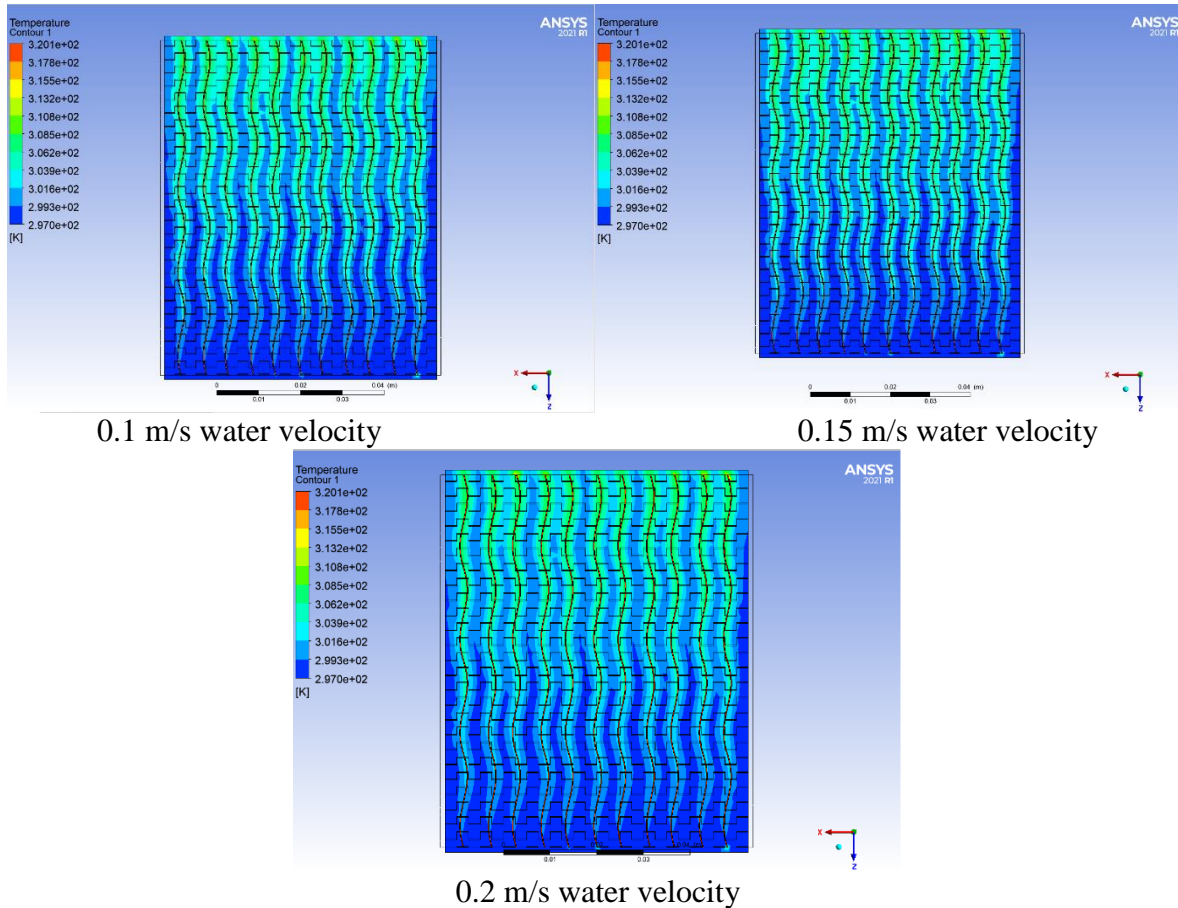



Figure 5: Temperature contours for heat exchanger using 50 oC water temperature, 3 m/s air velocity, 25 oC air temperature, and different values of water velocities.

On both sides of the fins, there are clearly forming thermal boundary layers giving a layered appearance to the temperature distribution. In contrast, the downstream fluid's temperature distribution is more uniform in the three serrated fin structure models because of the fins' serrated pattern. The contours make it abundantly evident that the downstream fin would disrupt the relatively uniform high temperature distribution in the area between the upstream parallel fins. This would result in the formation of new thermal boundary layers and a stronger heat transfer between the fluid and the fin. The figures illustrate that the serrated fin structure experiences a higher rate of temperature change than the plain fin structure. Additionally, as fin length decreases, there is a greater frequency of disturbances to the temperature distribution, which is

responsible for the increased rates of temperature change and temperature differences of fluids between the inlet and outlet. The data makes it evident that, under lower load conditions, there is a faster rate of temperature change and a wider temperature difference between the input and the output. Low load conditions have lower inlet average velocities than high load conditions, which results in longer fluid flow times over the entire model. This promotes the development of the temperature field and more adequate heat transfer. As depicted in Figures, the downstream region's temperature distribution is noticeably uniform under lower load conditions, with the exception of the faster temperature shift. Furthermore, at all load conditions, there are tail-like high-temperature regions between neighboring fins. These regions' length is significantly shorter under

* Corresponding author E-mail address: Laith.J.Habeeb@uotechnology.edu.iq
<https://doi.org/10.61268/qe48kc51>

This work is an open-access article distributed under a CC BY license
 (Creative Commons Attribution 4.0 International) under

<https://creativecommons.org/licenses/by-nc-sa/4.0/> 

lower stress conditions, presumably because of the temperature field developing more

sufficiently.

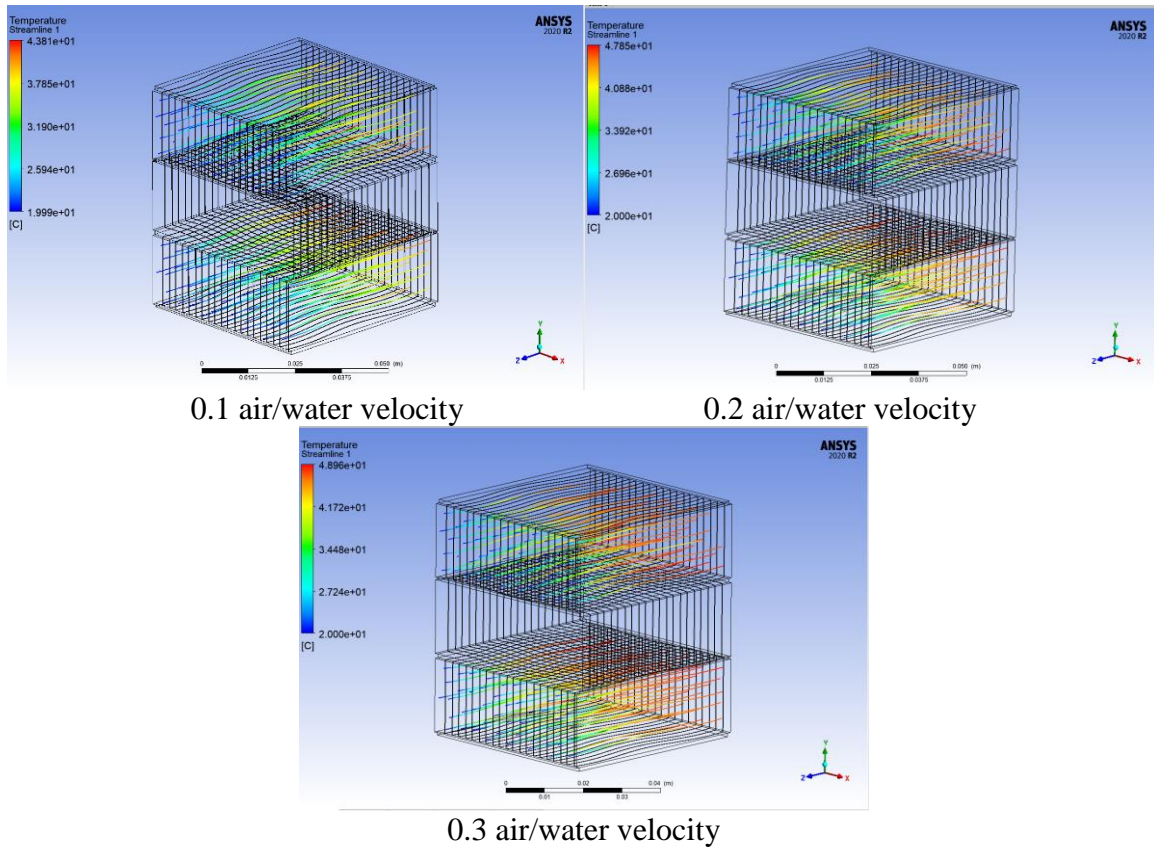
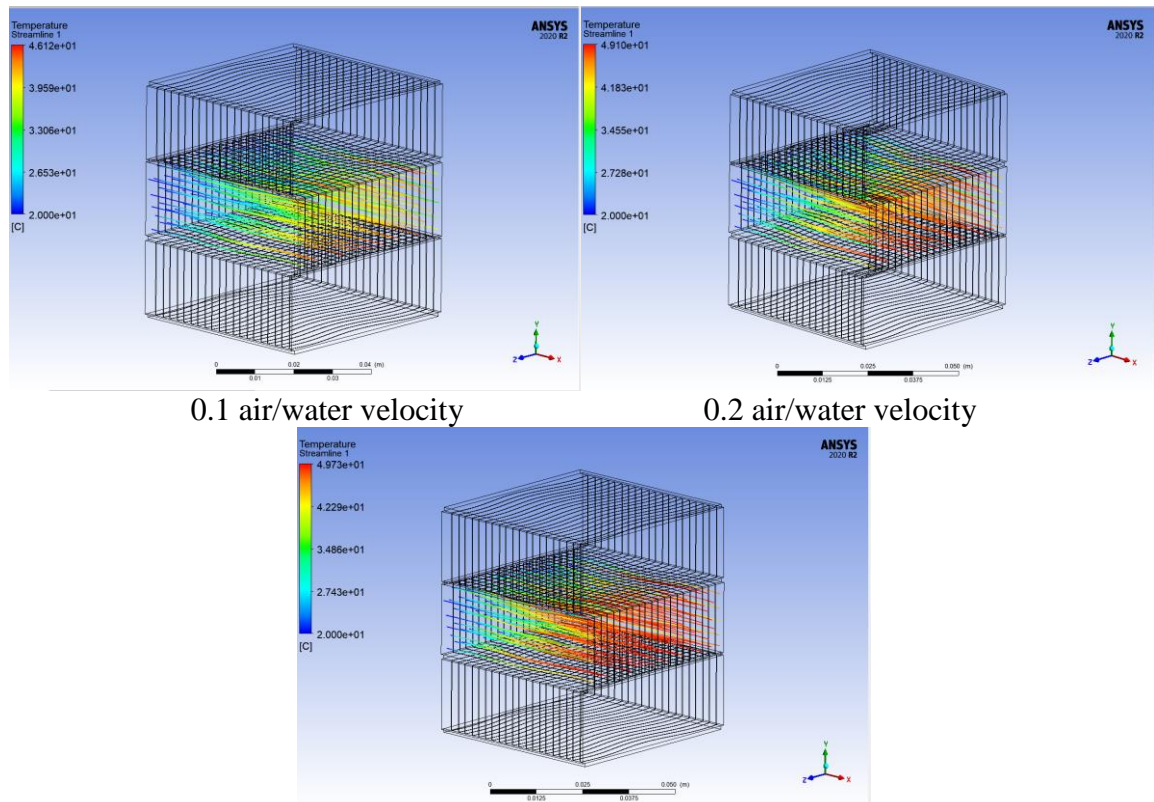
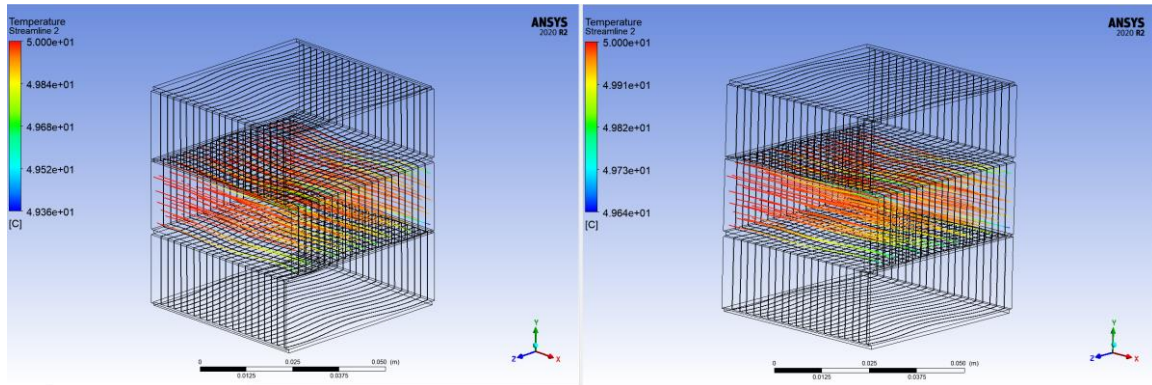


Figure 6: Temperature streamline for heat exchanger with external side air and water at the middle taken at 20 fins wavelength and 0.2 mm fin thickness.



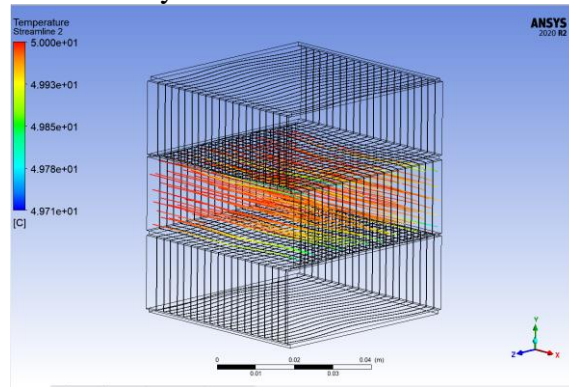
0.3 air/water velocity

Figure 7: Temperature streamline for heat exchanger with external side water and air at the middle taken at 20 fins wavelength and 0.2 mm fin thickness.



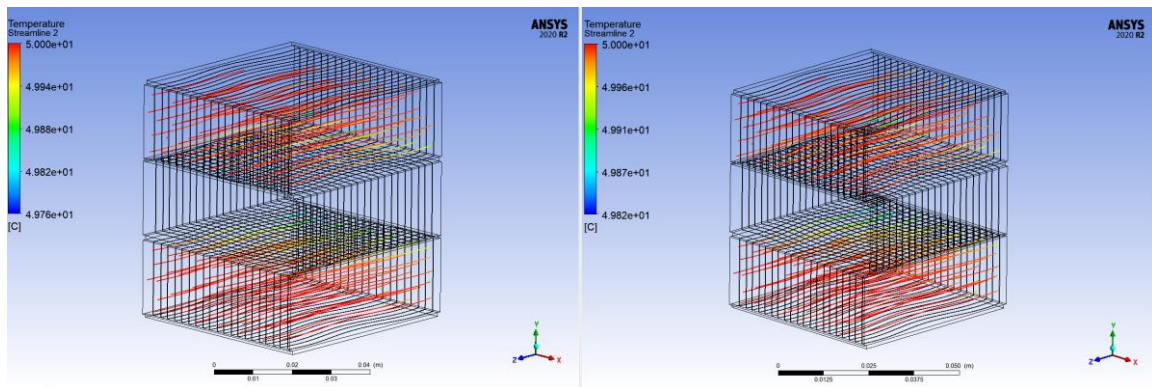
0.1 air/water velocity

0.2 air/water velocity



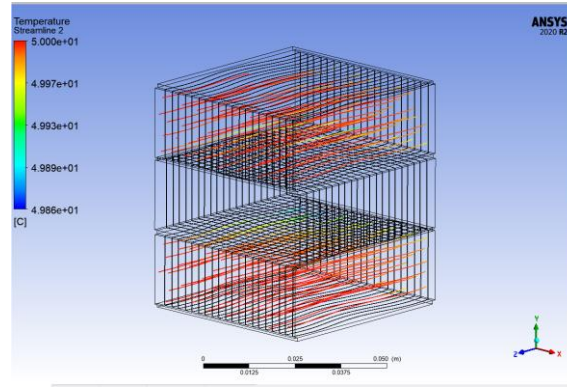
0.3 air/water velocity

Figure 8: Temperature streamline for heat exchanger with external side air and water at the middle taken at 20 fins wavelength and 0.2 mm fin thickness.



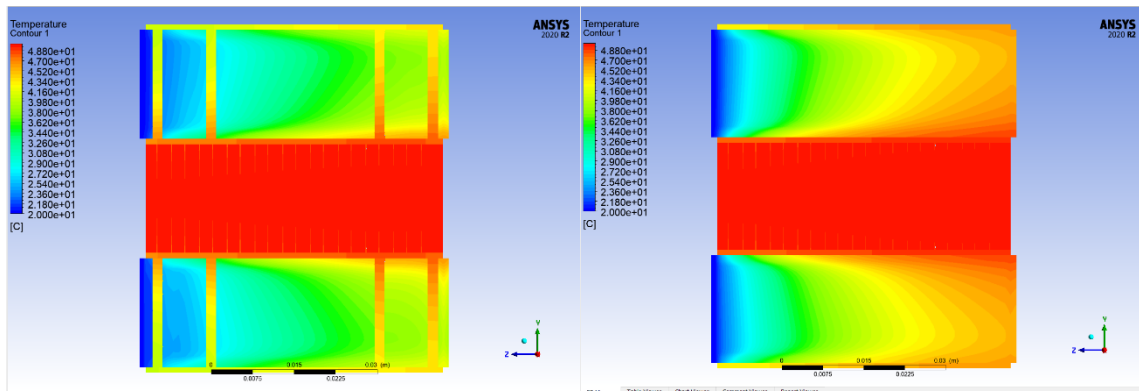
0.1 air/water velocity

0.2 air/water velocity

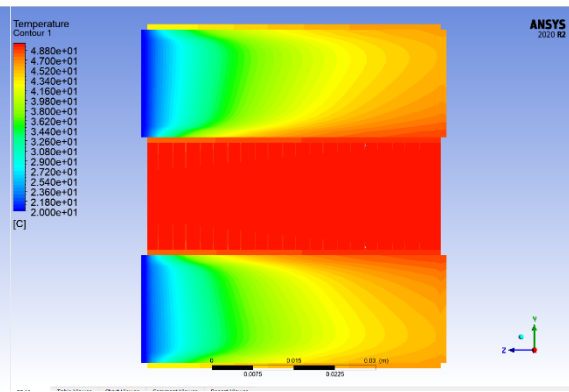


0.3 air/water velocity

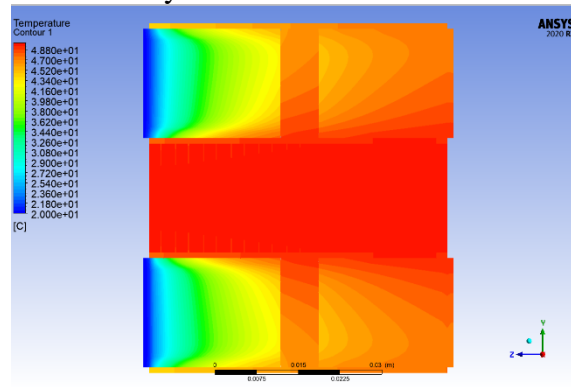
Figure 9: Temperature streamline for heat exchanger with external side water and air at the middle taken at 20 fins wavelength and 0.2 mm fin thickness.



0.1 air/water velocity



0.2 air/water velocity



0.3 air/water velocity

Figure 10: Temperature contour for heat exchanger with external side air and water at the middle taken at 20 fins wavelength and 0.2 mm fin thickness.

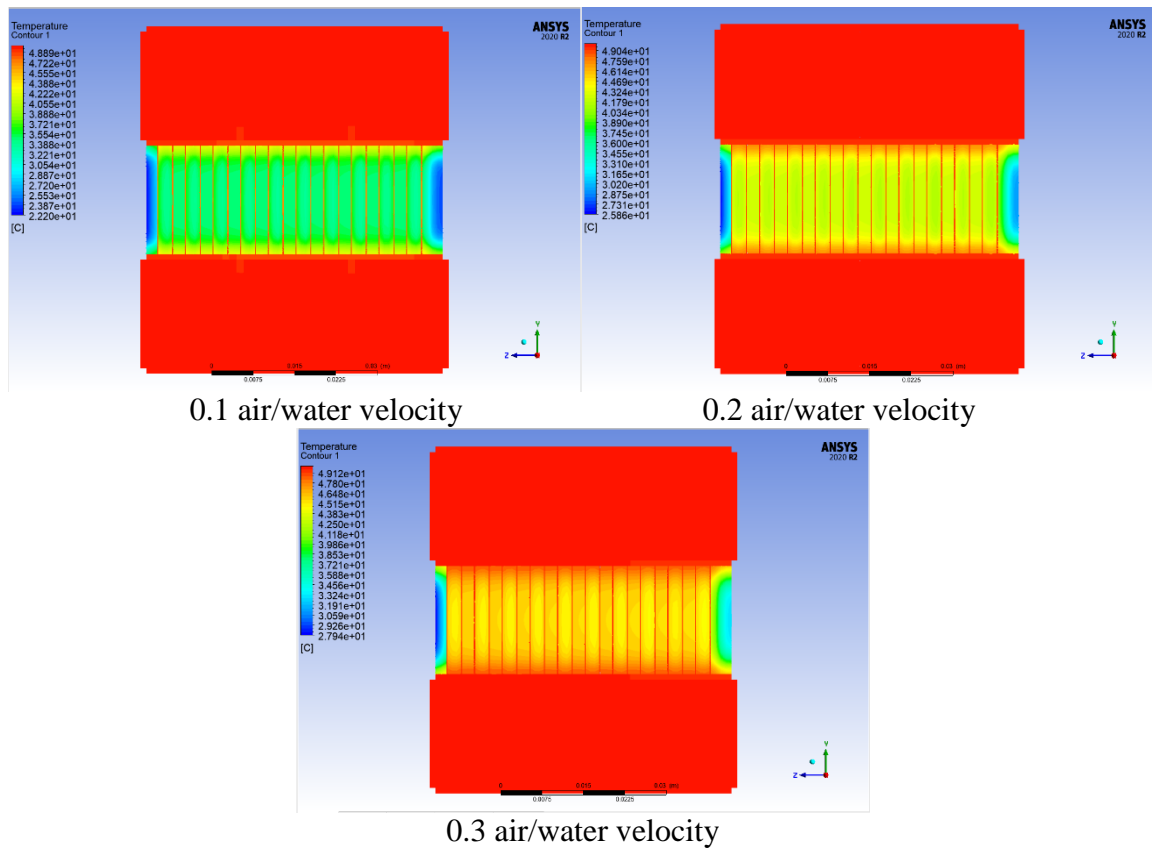


Figure 11: Temperature contour for heat exchanger with external side water and air at the middle taken at 20 fins wavelength and 0.2 mm fin thickness.

4.2 Velocity Distribution

The heat exchanger's velocity contours are displayed in Figures (12) and (13) as the water's velocity varies. Specifically, water was the working medium. It is evident that the flow has a periodic feature in the direction of flow. At the junction of two fins, the fluid's velocity increases noticeably. A low-speed zone forms between two adjacent fins in the flow direction as a result of the fins' blockage. Consequently, the fluid straight flow channel presents a clear, relatively high-speed zone. Additionally, a reversal in the fluid flow is found close to the fins as a result of backpressure backflow. The primary source of the backpressure backflow is an increase in downstream pressure above the system pressure.

Because of the fully established velocity condition at the intake, it is evident that the velocity distribution does not alter along the direction of flow. On the other hand, the

double peak feature is clearly seen in the velocity distributions for the serrated fin. Due to the fins' serrated arrangement, fluids' cross-sectional shapes vary along the z-coordinate. The downstream fin will split the fluid between two neighboring parallel fins into two sections. The low-valley section of the velocity curve of the structure with serrated fins corresponds to the fluid's velocity decreasing in the middle region when the fluid is ready to bump against the fin due to the fin's resistance. Low-valley sections can also be caused by the flow velocity being substantially lower in the middle of the forepart region between two adjacent parallel fins, which is caused by the upstream fin's shielding effect. Additionally, the fluid in the upstream zone would be split into two halves due to the fins' serrated arrangement, and the majority of the fluid would travel aside the downstream fins, which corresponds to the double peak portion in the velocity distribution.

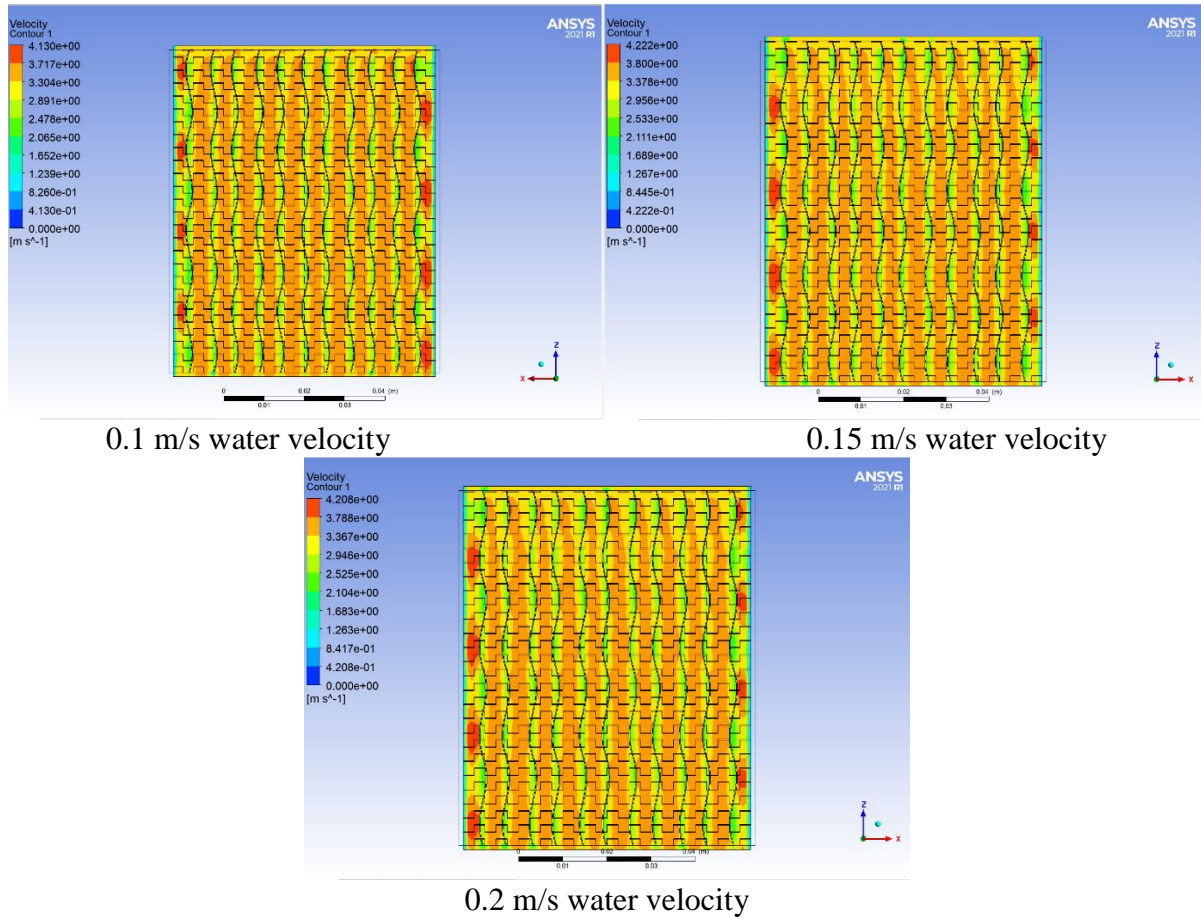
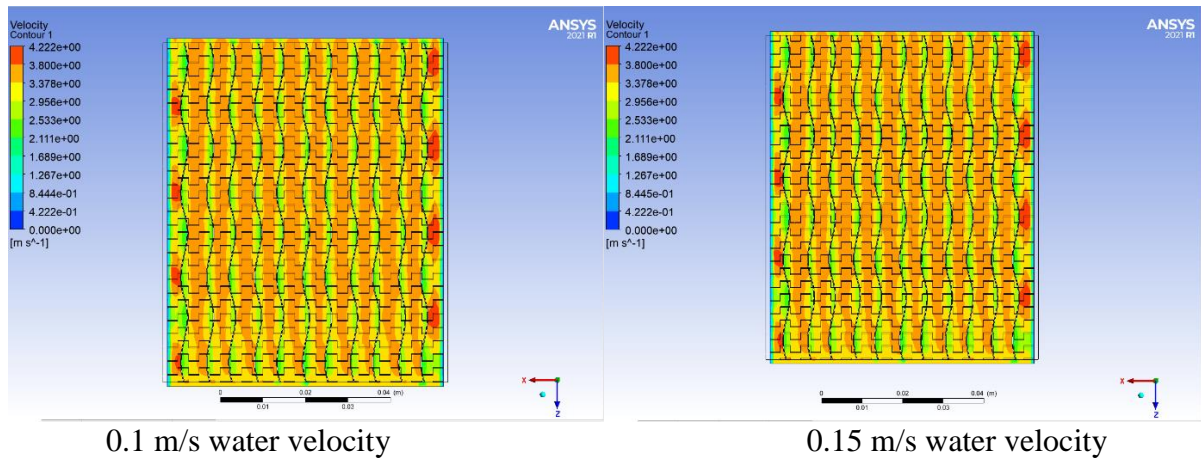
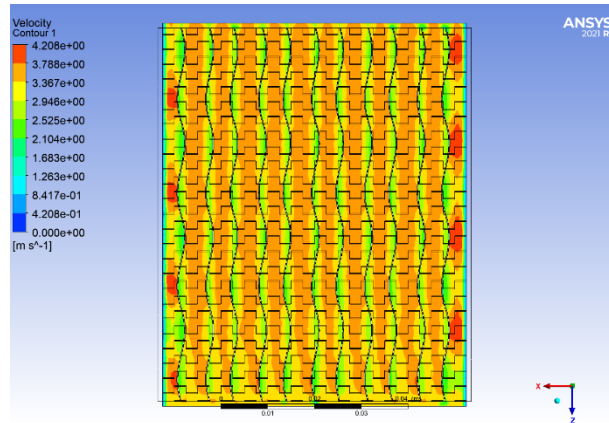


Figure 12: Velocity contours for heat exchanger using 25 °C water temperature, 3 m/s air velocity, 50 °C air temperature, and different values of water velocities.





0.2 m/s water velocity

Figure 13: Velocity contours for heat exchanger using 50 °C water temperature, 3 m/s air velocity, 25 °C air temperature, and different values of water velocities.

It's crucial to note that the velocity distribution statistics in the figures were taken from several models at the same position. Hence, while the flow lengths from the head of a single fin to the data points are different, the flow distances between the downstream fin and data points are the same in the flow direction. The velocity distribution is likely closer to a fully developed distribution and will be greater in the center position of the channel, as indicated by the longer flow distance from the entrance. As a result, the velocity curve's minimum value is biggest. Additionally, as the figures show, the high velocity fluid concentrates in the two side areas of a single fin forepart due to the guiding influence of nearby fins on the fluid. Furthermore, the shorter fin structure has a stronger directing impact on the fluid flow due to the concentration behavior of the high-velocity fluid near the fin being more visible.

Due to the completely developed velocity dispersion in the inlet, the boundary layer velocity stays constant. In contrast, the velocity curves for the three models with serrated fins show clear periodic oscillations. Every segment between two velocity peaks for each wavy curve represents the velocity distribution in the boundary layer of a single fin. The channel contraction brought on by the thickness of the fin and the fluid's acceleration is the reason for the quick increase in velocity in the first part of the three curves. On the other hand, the velocity growing in the channel is what causes the velocity reduction in the final segment of the

three curves. With the exception of the first and last, all subsequent portions share the same characteristics: the velocity initially lowers and then increases, indicating periodic destruction of the boundary layer as a result of the fins' serrated arrangement. Furthermore, the velocity in the serrated fin's boundary layer is higher than that of the plain fin, indicating that the serrated fin's boundary layer is thinner than that of the plain fin, which is advantageous for heat transfer.

5. Conclusions

Using CFD study with FLUENT 2020 R1, the performance characteristics of the compact plate fin heat exchanger's improved surfaces are examined. Data from earlier research is used to validate the CFD predictions. The geometrical characteristics of the three-dimensional fin flow channel are described. Heat transfer and flow friction correlations covering a broad range of Reynolds number, including the full laminar and turbulent regions, were obtained by simulating the flow and temperature fields in plate fin heat exchanger. The pressure, temperature, and velocity contours were taken from the Fluent simulations.

1. It was discovered that when the velocities of the air and water rise, so does the pressure inside the heat exchanger.
2. The temperature distribution's outlines which show how the temperature inside the heat exchanger varies with variations in the air and water intake temperatures.

3. Because the topmost layer is part of a warm stream's flow channel, the temperature rises there, while the bottom layer exhibits the reverse effect because it is part of a cold stream's flow passage.
4. As the thickness of the fin increases, the area of solid in the staggered position's longitudinal section increases as well. This strengthens the fluid's turbulence at the staggered position, increasing the local resistance loss there.
5. Changes in fluid temperature in the depth direction are caused by convection heat transfer to the surroundings and conduction heat transfer via the heat exchanger's side plates.
6. Because of the fully established velocity condition at the intake, it is evident that the velocity distribution does not alter along the path of flow.

References

- [1] Fehle, R., J. Klas, and F. Mayinger. "Investigation of local heat transfer in compact heat exchangers by holographic interferometry." *Experimental thermal and fluid science* 10.2 (1995): 181-191.
- [2] Ranganayakulu, Ch, K. N. Seetharamu, and K. V. Sreevatsan. "The effects of longitudinal heat conduction in compact plate-fin and tube-fin heat exchangers using a finite element method." *International journal of heat and mass transfer* 40.6 (1997): 1261-1277.
- [3] Hajabdollahi, Hassan, Mojtaba Tahani, and MH Shojaei Fard. "CFD modeling and multi-objective optimization of compact heat exchanger using CAN method." *Applied Thermal Engineering* 31.14 (2011): 2597-2604.
- [4] Pingaud, H., Le Lann, J. M., Koehret, B., & Bardin, M. C. (1989). Steady-state and dynamic simulation of plate fin heat exchangers. *Computers & Chemical Engineering*, 13(4), 577-585.
- [5] Müller-Menzel, T., and T. Hecht. "Plate-fin heat exchanger performance reduction in special two-phase flow conditions." *Cryogenics* 35.5 (1995): 297-301.
- [6] Dubrovsky, E. V. "Experimental investigation of highly effective plate-fin heat exchanger surfaces." *Experimental thermal and fluid science* 10.2 (1995): 200-220.
- [7] Ranganayakulu, Ch, K. N. Seetharamu, and K. V. Sreevatsan. "The effects of inlet fluid flow nonuniformity on thermal performance and pressure drops in crossflow plate-fin compact heat exchangers." *International Journal of Heat and Mass Transfer* 40.1 (1996): 27-38.
- [8] Kundu, B., and P. K. Das. "Optimum dimensions of plate fins for fin-tube heat exchangers." *International journal of heat and fluid flow* 18.5 (1997): 530-537.
- [9] Ranganayakulu, Ch, and K. N. Seetharamu. "The combined effects of longitudinal heat conduction, flow nonuniformity and temperature nonuniformity in crossflow plate-fin heat exchangers." *International communications in heat and mass transfer* 26.5 (1999): 669-678.
- [10] Picon-Nunez, M., G. T. Polley, E. Torres-Reyes, and A. Gallegos-Munoz. "Surface selection and design of plate-fin heat exchangers." *Applied Thermal Engineering* 19, no. 9 (1999): 917-931.
- [11] Wen, Jian, and Yanzhong Li. "Study of flow distribution and its improvement on the header of plate-fin heat exchanger." *Cryogenics* 44.11 (2004): 823-831.
- [12] Şahin, B., A. Akkoca, N. A. Öztürk, and H. Akilli. "Investigations of flow characteristics in a plate fin and tube heat exchanger model composed of single cylinder." *International journal of heat and fluid flow* 27, no. 3 (2006): 522-530.
- [13] Peng, Hao, and Xiang Ling. "Optimal design approach for the plate-fin heat exchangers using neural networks cooperated with genetic algorithms." *Applied Thermal Engineering* 28.5 (2008): 642-650.
- [14] Manglik, R. M., & Bergles, A. E. (1995). Heat transfer and pressure drop correlations for the rectangular offset strip fin compact heat exchanger. *Experimental Thermal and Fluid Science*, 10(2), 171-180.
- [15] Mishra, Manish, P. K. Das, and Sunil Sarangi. "Second law based optimisation of crossflow plate-fin heat exchanger design using genetic algorithm." *Applied thermal engineering* 29.14 (2009): 2983-2989.
- [16] Ismail, L. Sheik, Ch Ranganayakulu, and Ramesh K. Shah. "Numerical study of flow patterns of compact plate-fin heat exchangers and generation of design data for offset and wavy fins." *International journal of heat and mass transfer* 52.17 (2009): 3972-3983.
- [17] Suzuki, K., E. Hirai, T. Miyake, and T. Sato. "Numerical and experimental studies on a two-dimensional model of an offset-strip-fin type compact heat exchanger used at low Reynolds number." *International journal of heat and mass transfer* 28, no. 4 (1985): 823-836.
- [18] Youcef-Ali, Sabri. "Study and optimization of the thermal performances of the offset rectangular plate fin absorber plates, with various glazing." *Renewable Energy* 30.2 (2005): 271-280.
- [19] Schulte-Fischedick, Jan, Volker Dreißigacker, and Rainer Tammé. "An innovative ceramic high temperature plate-fin heat exchanger for EFCC processes." *Applied Thermal Engineering* 27.8 (2007): 1285-1294.
- [20] [18]A. . Abdulnabi Lazim, . A. . Daneh-Dezfuli, and L. HABEEB, "Magnetic Field Impact on Heat

Transfer and Nano-Ferrofluid Flow in a Pipe”, Rafidain J. Eng. Sci., vol. 2, no. 1, pp. 82–98, Dec. 2023, <https://doi.org/10.61268/vxe63398>.

- [21] M. . Abdulritha Khazaal, A. . Daneh-Dezfuli, and L. HABEEB, “Investigation the thermal performance of Nano-Enhanced Phase Change Material (NEPCM) in

an enclosure”, Rafidain J. Eng. Sci., vol. 2, no. 1, pp. 107–118, Jan. 2024,

<https://doi.org/10.61268/s7wgnk73>.